



Article ID 1007-1202(2022)05-0424-15

DOI <https://doi.org/10.1051/wujns/2022275424>

# Back Frame Optimization of a Large Radio Telescope Based on Force Cone Method

□ **WU Qinglong, YAO Zhan, WU Tanhui,  
FANG Houfei, HOU Yangqing**

Shanghai YueSheng Information Technology Co., Shanghai  
201108, China

© Wuhan University 2022

**Abstract:** A new research perspective is proposed to optimize the topology of truss structure by force cone method, which involves force cone drawing rules and growth rules. Through the comparison with the mature variable density topology optimization method, the effectiveness of force cone method is verified. This kind of new method is simple and easy to understand (no need to master complex structural optimization design theory). Besides, it is time-saving in finite element calculations, and can obtain an optimized truss layout easily. By drawing the force cone, its application on a large radio telescope's back frame structure shows that, compared with the existing one in terms of structural stiffness, Root Mean Square (RMS) precision, and beam stress distribution, the optimized back frame using the force cone method has higher stiffness, better RMS, more uniform stress, and lighter weight.

**Key words:** large radio telescope; back frame; force cone method; topology optimization

**CLC number:** TH 11

**Received date:** 2022-03-25

**Biography:** WU Qinglong, male, Ph.D., research direction: structural optimization. E-mail: wql499451368@163.com

## 0 Introduction

As the skeleton of main reflecting surface, the back frame structure is the most important part of a large radio telescope. Its own weight load has a great impact on the precision of the telescope. Optimization design of the back frame structure can reduce the structural weight and improve the Root Mean Square (RMS) precision of the telescope. von Hoerner<sup>[1]</sup> proposed the homologous design for telescope in 1967. The main idea of homologous design can be summarized as follows: the back frame structure deforms under the load of its own weight. First, find the best matching paraboloid of the deformed reflecting surface; then set the best matching paraboloid as the deformed reflecting surface and thus the displacement value of each point on the reflecting surface is calculated; finally, optimize the beam cross-section until the deformation of the telescope structure meets the displacement value. Chen *et al*<sup>[2]</sup> proposed the accurate homologous design, in which the relative precision of reflecting surface can reach the extreme by satisfying the relative error of the reflective surface with zero RMS. Levy<sup>[3]</sup> explored the use of segmented search method and the virtual power/lagrangian multiplier method to optimize the telescope structure. Liu *et al*<sup>[4,5]</sup> introduced genetic algorithms in the cross-section optimization of the Xinjiang 110m All-Movable Telescope, and improved the electrical performance of the telescope.

Topology optimization is a popular research topic in the field of structure optimization. At present, the widely used methods include variable density method

(VDM), Evolutionary Structural Optimization (ESO), Soft Kill Option (SKO), ground structure method and so on<sup>[6]</sup>. There are also some emerging topology optimization methods, such as moving morphable components<sup>[7,8]</sup>, cellular division method<sup>[9]</sup> and topology optimization method based on bone remodeling theory<sup>[10]</sup>. These optimization methods often require users to master the theory of structural optimization algorithms, finite element methods and be proficient in optimization and calculation software. In addition, some methods also require users to master more complex artificial intelligence theory, bone remodeling theory and image processing algorithms. Thus, the threshold is extremely high. Based on the idea of force cone, this paper proposes a force cone growth method for optimizing the topology of truss structures. Compared with the traditional methods, the force cone growth method is simple and easy to understand. There is no need to master the complex structural optimization theory nor to require time-consuming finite element calculation. The optimized truss layout can be easily obtained by drawing the force cone of constraints and loads by graphical method. As a new method for the optimization of truss structures, the force cone growth method is simple in theory, effective in method and has low requirements for users. It can quickly obtain the optimized layout of truss structure and provide a new idea for structural topology optimization.

Most traditional telescope back frame structure adopts the circular cross spatial structure. Liu<sup>[11]</sup> adopted a pyramid system spatial structure in the back frame structure, which generally presents two layers. The upper layer uses a triangular pyramid, while the lower layer uses a quadrangular pyramid. The reasonable combination of two kinds of pyramid makes the entire back frame structure more uniform, the arrangement of beams denser, and the force distribution better than that of the circular cross spatial structure. Qian *et al*<sup>[12]</sup> proposed a shape-keeping method for the back frame structure of FAST (Five-hundred-meter Aperture Spherical radio Telescope), providing and optimizing various back frame structures such as the spatial latticed structure, strain stressed structure, and hybrid structure. Zhao *et al*<sup>[13]</sup> optimized the FAST back frame structure, made a comparison of different structural forms, and made detailed parameter selections on the divided number of a back-structure side, tilt angle, section type and back frame structure height.

Essentially, the optimization of the telescope back frame is truss optimization, which mainly includes topology optimization and size optimization. Most of the research on truss topology optimization is based on the ground structure method<sup>[14,15]</sup>. Meanwhile, the full stress method is widely used for truss size optimization<sup>[16,17]</sup>. In this paper, the research on the back frame topology optimization of a large radio telescope is carried out based on a new research perspective—force cone. Through this force cone growth method, an optimized topology of truss structure is proposed to obtain a high-precision and light weight in large radio telescope back frame structure.

## 1 Force Cone Method for Truss Topology Optimization

### 1.1 The Concept of Force Cone

Figure 1 shows the von Mises stress contour and principal stress contour under a radial load applied to the center of a circular area that fixed on all sides. The main stress is distributed in a 90° cone area. A pressure cone and a tension cone are formed before and after the force. This is the concept of force cone. Based on the force cone, Mattheck *et al*<sup>[18]</sup> proposed a new thinking tool for lightweight structures. Inspired by the work of Mattheck *et al*, this paper proposes the force cone growth method to optimize the layout of truss structure. This method does not require computer calculations, and the optimized truss layout can be obtained just by drawing. Besides, the design completed by this method performs more excellently in topology compared with the variable density method.

### 1.2 Drawing Rules of Force Cone

There are two kinds of force cone, namely the load force cone and the constraint force cone. Load force

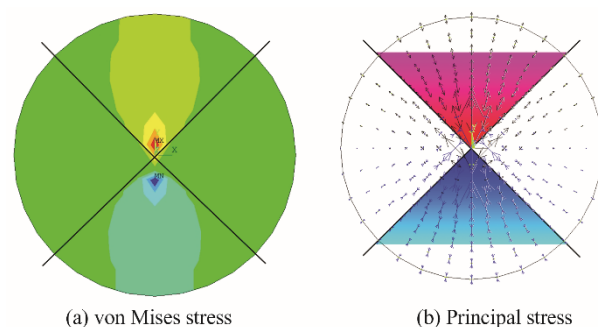


Fig.1 Concept of force cone

cone grows out from the point where load is applied, while the constraint force cone grows out from the constraint point. The followings are the drawing rules for the two force cones.

**Load force cone:** The load point is the origin of the force cone. The side in the same direction of the load is the pressure cone, and the side opposite to the load is the tension cone.

**Constraint force cone:** Assuming the load acts on the constraint point, the constraint point will generate a reaction force in the opposite direction of the load. Therefore, the orientation of the constraint force cone is the same as the load force cone, while its direction of the tension cone and pressure cone is opposite.

### 1.3 Growth Rules of Force Cone

The force cone is grown through the following steps .

- 1) Clarify design boundary conditions, including design domain, loads and constraints.
- 2) Draw the load force cones.
- 3) Draw the constraint force cones.
- 4) When the constraint point is inside (or at the boundary) of the load force cone and the connection line between the load point and the constraint point does not exceed the design domain, then directly connect the load point and the constraint point to form the beam.
- 5) For constraint points that do not meet the above conditions, extend the constraint force cones until the constraint force cones meet the load force cone or the boundary of the design domain.
- 6) If the constraint force cone and the load force cone intersect inside the design domain, the intersection point is regarded as the  $\alpha^0$  point. If two constraint force cones intersect inside the design domain, the intersection point is the  $\beta^0$  point. If the constraint force cone and the load force cone do not intersect in the design domain, the constraint force cone reaches the boundary of the design domain and forms the boundary  $\gamma^1$  point.

7) When the constraint force cone intersects with the load force cone to form an  $\alpha^0$  point or intersects with the boundary to form a  $\gamma^1$  point, it does not extend. When two constraint force cones intersect in the design domain to generate a  $\beta^0$  point, they continue to extend until an  $\alpha$ -type point or a  $\gamma$ -type point is generated.

8) The  $\gamma^1$  point is used as a new constraint point. When the  $\gamma^1$  point is not connected with the adjacent constraint point and will not intersect with the existing beam

after being connected, connect the  $\gamma^1$  point with the adjacent constraint point. Then draw the force cone based on this new constraint point ( $\gamma^1$  point) until it intersects with the load force cone. The  $\gamma$ -type points generated in this process are sequentially marked as first-level  $\gamma$ -type points  $\gamma^1$ , second-level  $\gamma$ -type points  $\gamma^2$ , and third-level  $\gamma$ -type points  $\gamma^3$ . The  $\beta$ -type points formed by the intersection of the force cones of the  $\gamma$ -type points are respectively denoted as  $\beta^1, \beta^2, \beta^3$ . The  $\alpha$ -type points formed by the intersection of the  $\gamma$ -type point force cone and load force cone are respectively denoted as  $\alpha^1, \alpha^2, \alpha^3$ , and so on.

9) One boundary of the load force cone will only generate an  $\alpha$ -type point with one side of the constraint force cone. When multiple  $\alpha$ -type points are generated on one side of the load force cone during the drawing process, the following processing rules are used: 1) If the  $\alpha$ -type points are of different levels, keep the one with higher level and delete those with lower level. If the deleted  $\alpha$ -type point is generated by a  $\gamma$ -type point, delete the  $\gamma$ -type point and its related growth path. 2) If the  $\alpha$ -type points are of the same level, keep the  $\alpha$ -type point closest to the load point and delete others.

10) After all the constraint force cones intersect with the load force cone, the beams are arranged along the relevant force cone boundary to form an initial truss.

11) When the constraint point (load point) is not connected with an adjacent point, and will not intersect with the existing beams after connection, then connect them with beam. When the load point is not connected to a constraint point and will not intersect with the existing member after connection, then connect them with beam. When the two boundaries on one side of the load cone both have  $\alpha$ -type points and will not intersect with existing beams after being connected, then connect them with beam.

12) Zero bar judgment. Figure 2 shows the two zero-bar situations. In this paper, only the situation (a) is regarded as the zero-bar and deleted. When the structure in the situation (b) is deformed, the beams ① and ②

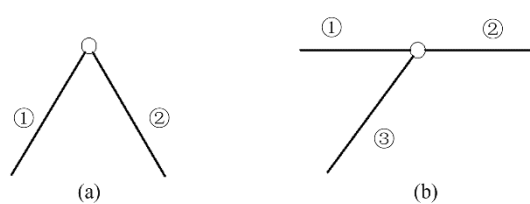


Fig. 2 Two situations of zero bar

will not be in a straight line and so the situation (b) is not regarded as a zero bar.

#### 1.4 Examples of Force Cone Method

Now we take some examples to illustrate the above force cone growth rules, and compare them with the results obtained by the classical variable density topology optimization method.

##### 1.4.1 Example 1

Example 1.1: Figure 3 shows the layout of constraints, load and the design domain. The length-to-height ratio of the design domain is 1:4. When the boundary conditions become clear, draw out the load force cone and the constraint force cones, as shown in

Fig.3 (b) and (c). It can be seen that the two constraint points are within the range of the load force cone, so directly connect the load point and two constraint points to generate a truss structure (growth rule 4), as shown in Fig.3 (d). Figure3(e) shows the result optimized by variable density method.

Example 1.2: As shown in Fig.4, it is the expansion of the design domain on the basis of Example 1.1. The length-to-height ratio of design domain is 1:2. At this time, the boundary of the load force cone and the constraint force cone coincide, and the truss structure is generated by arranging the beams along the boundary (growth rule 4).

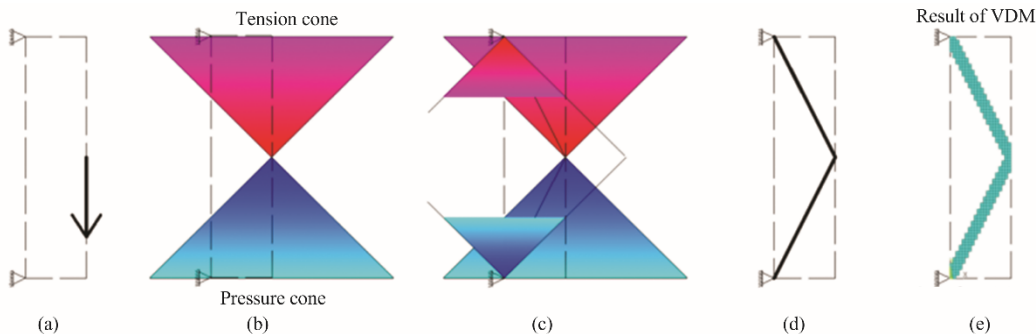


Fig. 3 Example 1.1 of the force cone method

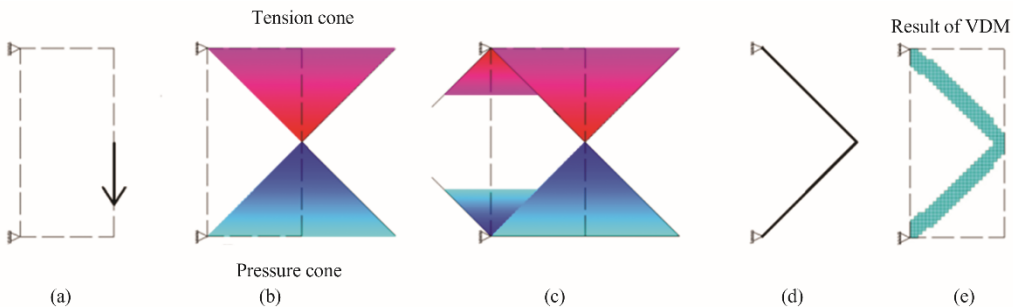


Fig. 4 Example 1.2 of the force cone method

Example 1.3: Continue to expand the design domain (Fig. 5). The length-to-height ratio of the design domain is 1:1, and the constraint points are out of the load force cone. First draw the load force cone (Fig. 5(b)); then draw the constraint force cones, and the constraint force cones intersect to generate  $\beta^0$  points (Fig. 5(c), growth rule 6). Continue to extend the constraint force cones and intersect them with load force cone to generate  $\alpha^0$  points (Fig. 5(d), growth rule 6). Arrange beams along the boundary of the relevant force cone to form an initial truss (Fig.5(e), growth rule 10). And finally connect the constraint points and adjacent points to form the final

truss (Fig.5(f), growth rule 11). Figure 5(g) shows the result optimized by variable density method.

Example 1.4: Again, continue to expand the design domain (Fig.6). The length-to-height ratio of the design domain is set as 2:1. First draw the load force cone (Fig. 6(b)). Then draw the constraint force cones. The constraint force cones intersect to generate  $\beta^1$  points, and intersect with the design domain boundary to generate  $\gamma^1$  points (Fig.6(c), growth rules 6, 7). Connect the  $\gamma^1$  points with the adjacent constraint points and use the  $\gamma^1$  points as the new constraint points and draw the new constraint force cones to intersect with the load force cone and gen-

erate  $\alpha^1$  points (Fig.6(d), growth rule 8). Finally arrange the beams along the boundary of the relevant force cone to form the initial truss (Fig. 6(e), growth rule 10) and connect the constraint points ( $\gamma^1$  points) with adjacent points to form the final truss (Fig.6(f), growth rule 11).

#### 1.4.2 Example 2

Example 2.1: On the basis of Example 1, change the load direction, reset the length-to-height ratio of design domain to 1:1, as shown in Fig. 7. At this time, the two constraint points are both within the range of the load force cone. The load point and the two constraint points are directly connected to generate a truss structure (growth rule 4).

Example 2.2: On the basis of Example 2.1, shrink the length-to-height ratio of the design domain to 1:2 (Fig. 8). At this time, the boundary of the load force cone and the constraint force cones coincide, and the truss structure is generated by arranging the beams along the boundary (growth rule 4).

Example 2.3: Continue to shrink the length-to-height ratio of the design domain to 1:4 (Fig. 9) and draw the load force cones and the constraint force cones. The original constraint force cones intersect with the boundary to generate 2  $\gamma^1$  points (Fig.9(b)). Redefine the  $\gamma^1$  points as the new constraint points and draw the new constraint force cones and intersect with the load force

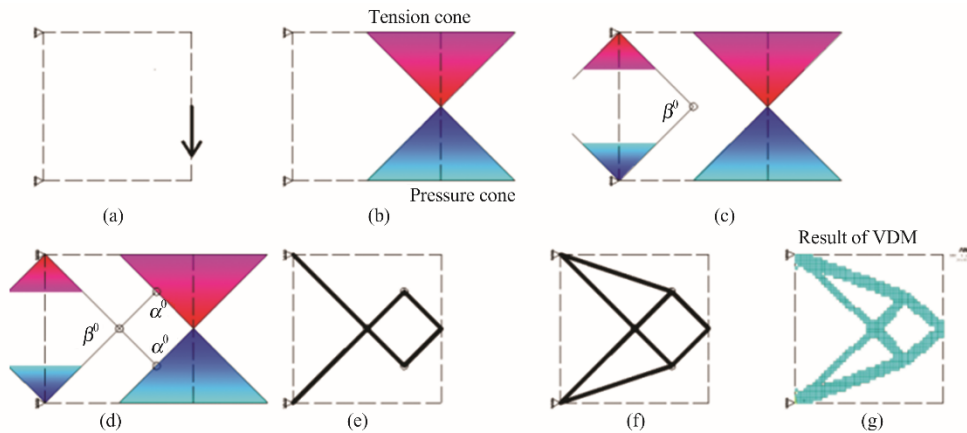


Fig. 5 Example 1.3 of the force cone method

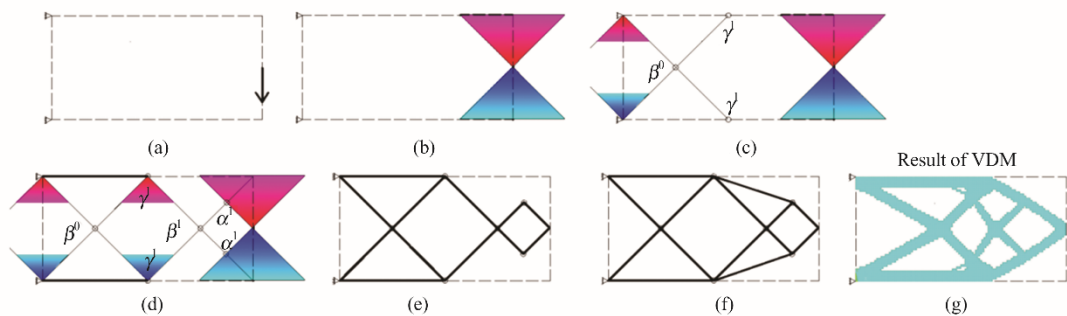


Fig. 6 Example 1.4 of the force cone method

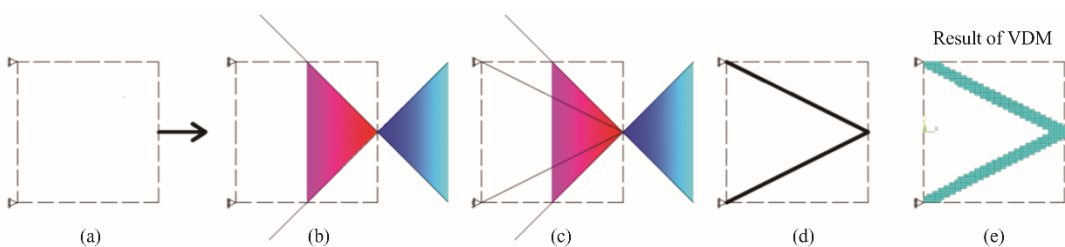


Fig. 7 Example 2.1 of the force cone method

cone to generate  $\alpha^1$  points (Fig. 9(c)). Arrange the beams along the boundary of the relevant force cone to form the initial truss. Finally connect the load point with the adjacent points, connect the constraint points with the adjacent points, and connect the two  $\alpha^1$  points of the force cone to obtain the optimized truss (Fig. 9(e)), growth rule 11).

#### 1.4.3 Example 3

Figure 10 is also a classic example in the field of structural optimization. The growth results of the force cone method are shown in Figs. 10 and 11 under different length-to-height ratio of 2:1 and 4:1, respectively.

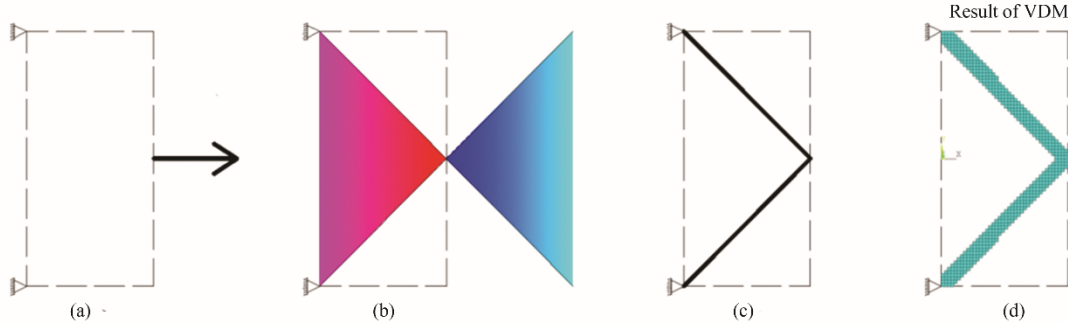


Fig. 8 Example 2.2 of the force cone method

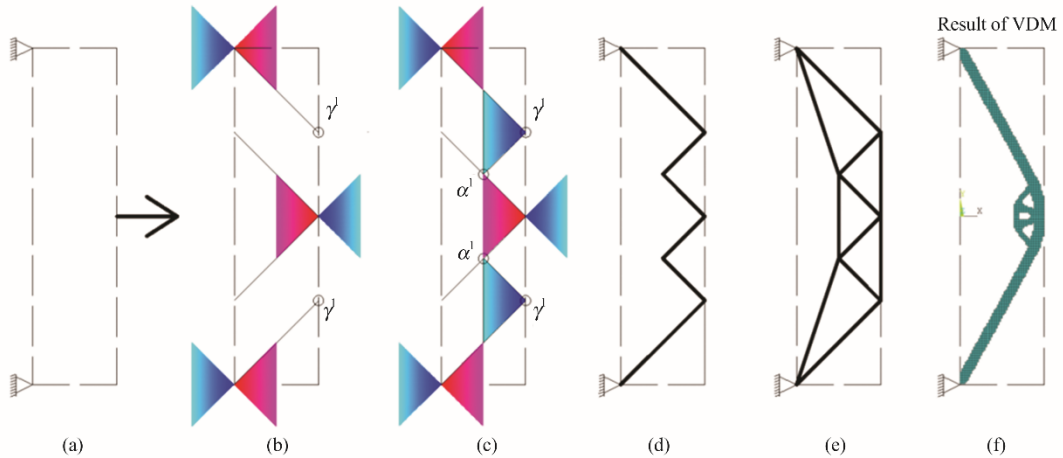


Fig. 9 Example 2.3 of the force cone method

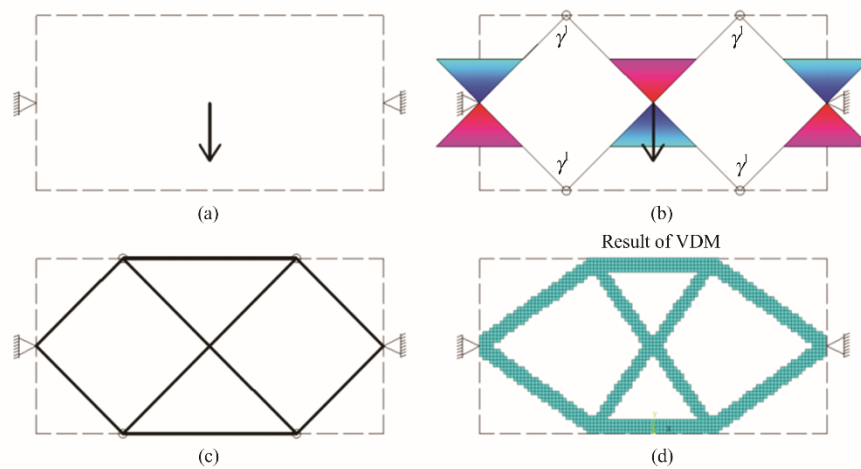


Fig. 10 Example 3.1 of the force cone method

#### 1.4.4 Some other examples

Figures 12-16 show some other examples of the force cone method. In these examples, the growth method is the same as the above example. While in these examples, the loads and constraints are not symmetrical,

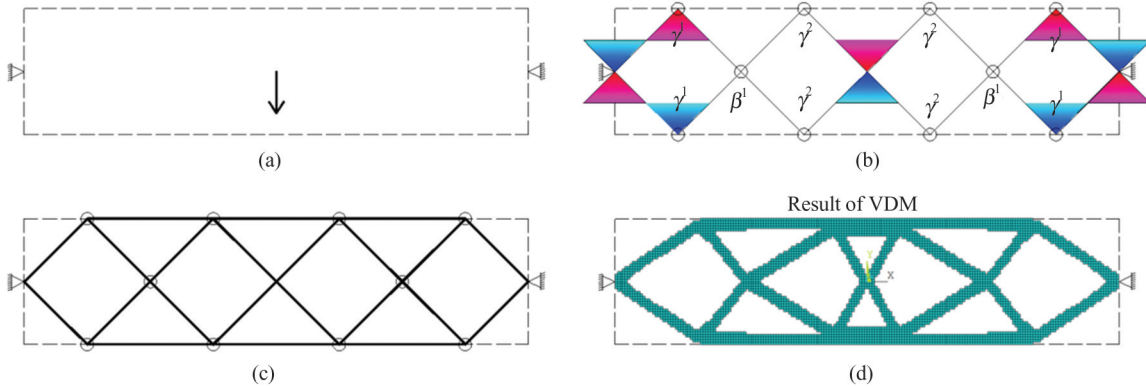


Fig.11 Example 3.2 of the force cone method

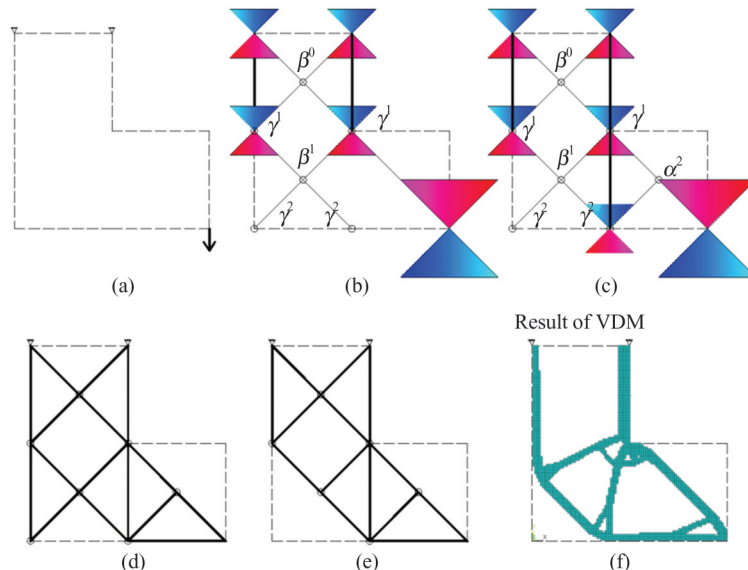
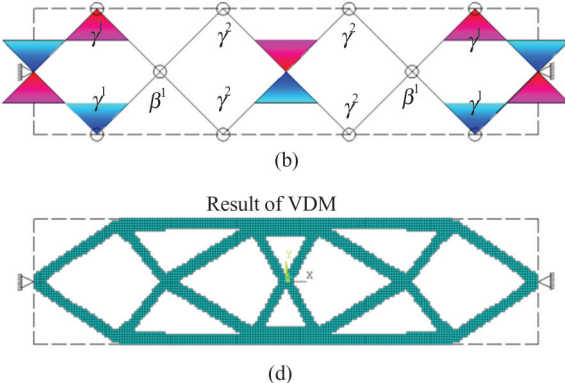


Fig.12 Example 4 of the force cone method

#### 1.4.5 Example of multi-load case force cone growth method

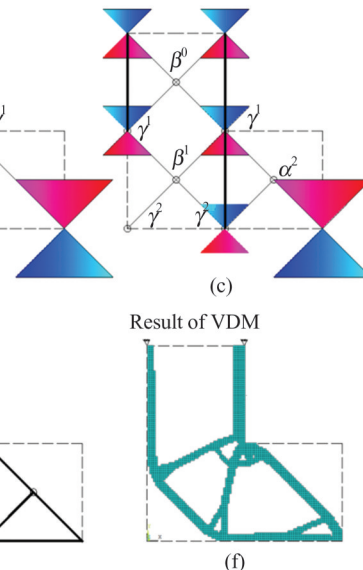
When multiple loads are applied to the structure, the force cone growth method is basically the same as that of a single load. It should be noted that the constraint force cone must grow to intersect with each load force cone. When two load force cones intersect, it is the same as the constraint force cones intersect, generating a  $\beta$ -type point. The following are several examples of force cone method when multiple loads are applied (Figs.17 and 18).

and the boundary conditions are more complicated. In addition, after obtaining the initial truss, there may be zero bars in some structures, and zero bars need to be deleted, as shown in Fig.12(d)-(e), Fig.13(d)-(e) (Growth Rule 13).



Result of VDM

(d)



Result of VDM

(f)

As shown in Fig.17(a), the length-to-height ratio of the design domain is 2:1. There are two constraint points on the left side of the design domain, and two loads applied to the middle and right sides of the lower side. As shown in Fig.17(b), first draw the load force cones and constraint force cones. The two constraint force cones intersect to form a  $\beta^0$  point, which is also an  $\alpha^0$  point generated by the intersection of the  $F_2$  load force cone and the  $C_2$  constraint force cone. Continue to extend the constraint force cones, which grow to intersect with the  $F_1$  force cone at points  $\gamma^1$  and  $\alpha^1$ , and  $\alpha^1$  is also the  $\beta^0$  point

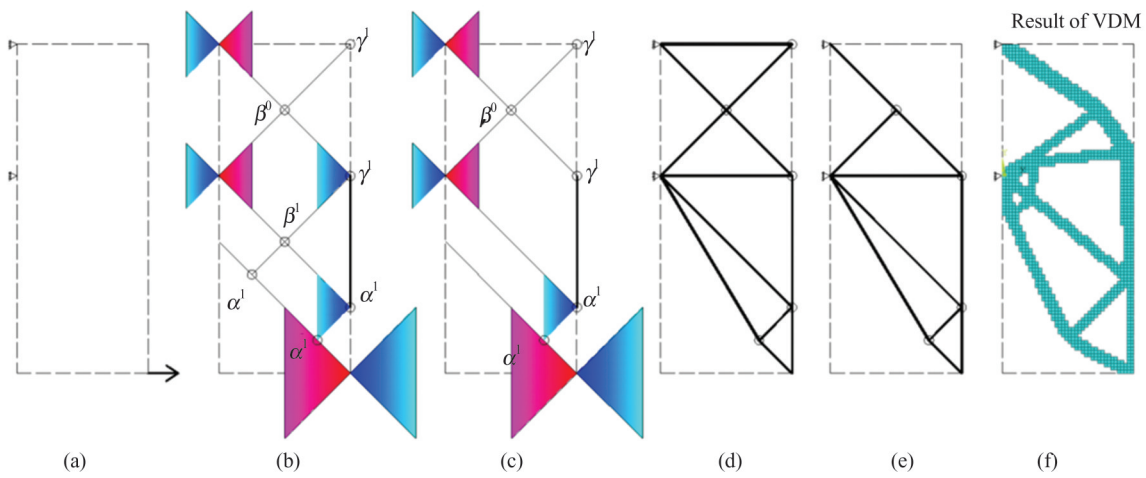


Fig. 13 Example 5 of the force cone method

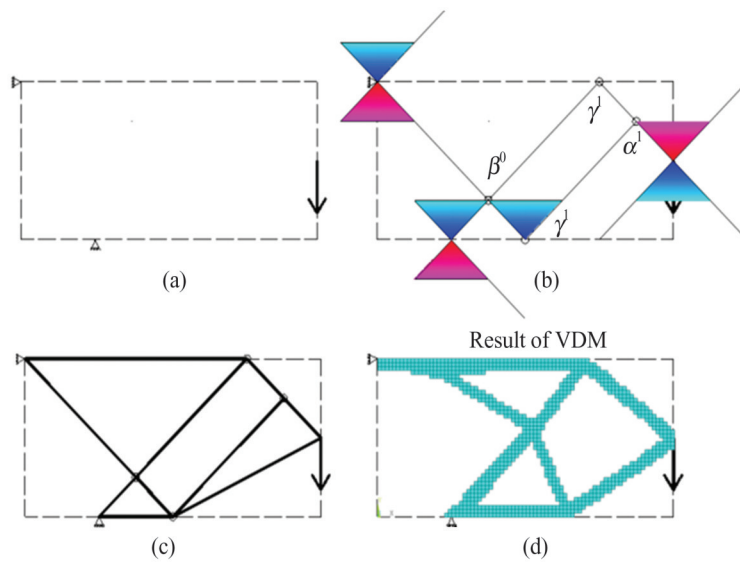


Fig. 14 Example 6 of the force cone method

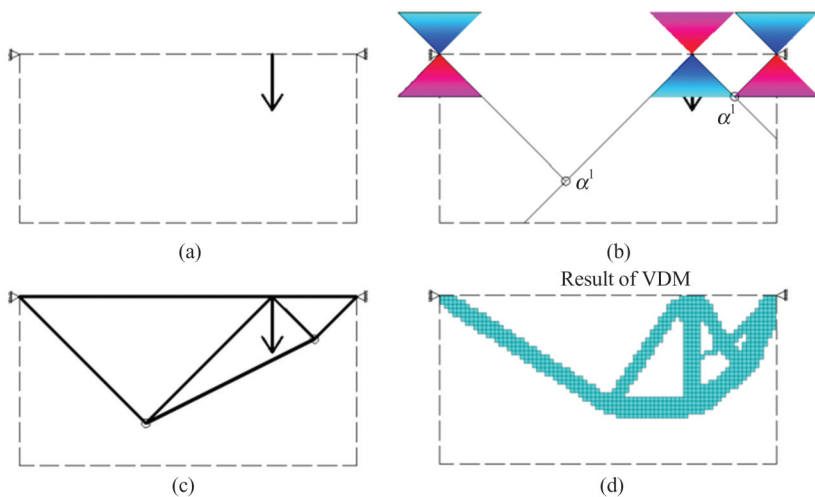


Fig. 15 Example 7 of the force cone method

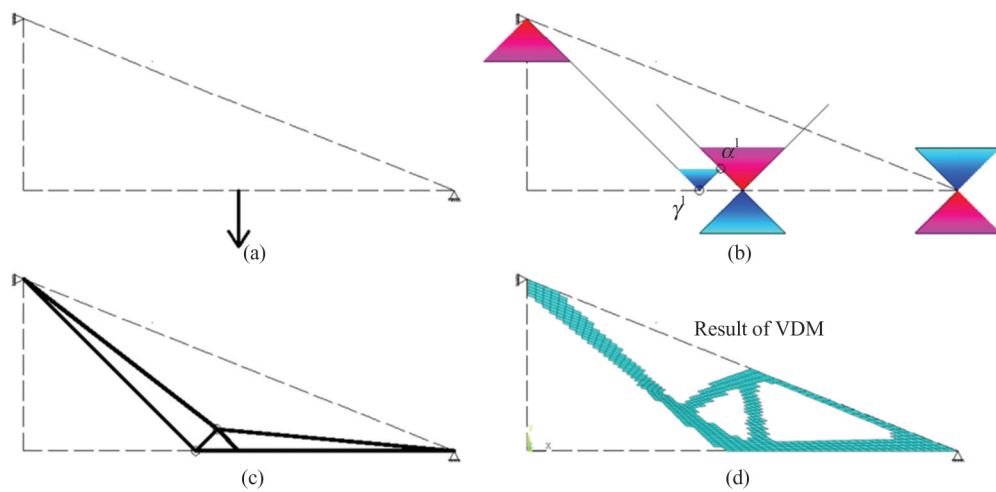


Fig. 16 Example 8 of the force cone method

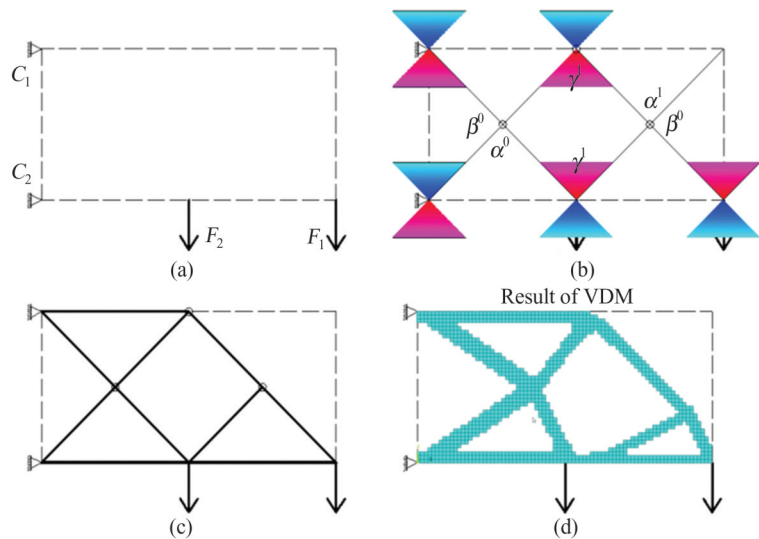


Fig. 17 Multiple loads example 1 of the force cone method

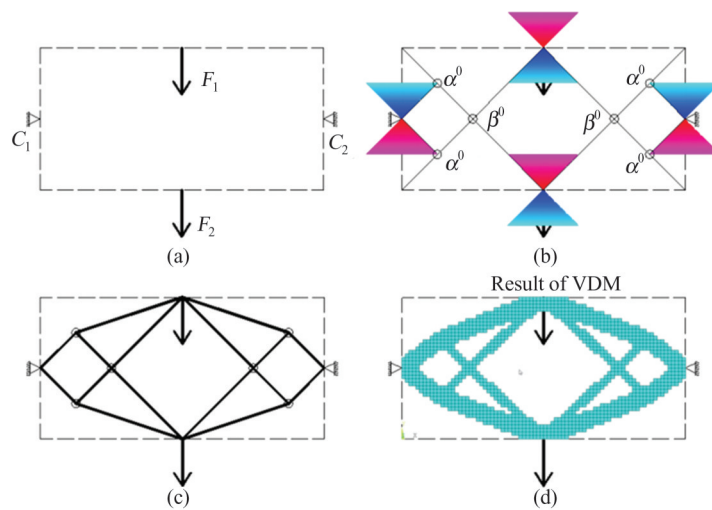


Fig. 18 Multiple loads example 2 of the force cone method

where the two load force cones intersect. The optimized structures obtained by the force cone growth method and the variable density method are shown in Fig. 17.

As shown in Fig. 18(a), the length-to-height ratio of the design domain is 2:1. The force cone growth process is shown in Fig. 18 (b). The two load force cones firstly intersect at two  $\beta^0$  points, and then intersect with the constraint force cone at four  $\alpha^0$  points.

### 1.5 Summary of Force Cone Growth Method

It can be seen from the above examples that the force cone growth method can obtain good truss layout under simple structural boundary conditions, which is very close to the optimization result of the classical variable density method, and the effectiveness of the force cone growth method is proved. However, this paper just makes a preliminary exploration of the force cone growth method, and the application of this method under complicated boundary conditions needs further research.

## 2 Back Frame Design of Large Telescope Based on Force Cone Method

As shown in Fig. 19, the back frame structure of a large radio telescope is complicated. But from a design point of view, the back frame is a rotationally symmetric structure composed of 32 identical portions. So optimization is only needed to be carried out for one of them. Taking one more step further, the frame structure design can be simplified to a plane.

### 2.1 Design of Existing Back Frame A

Figure 20 shows the existing back frame structure

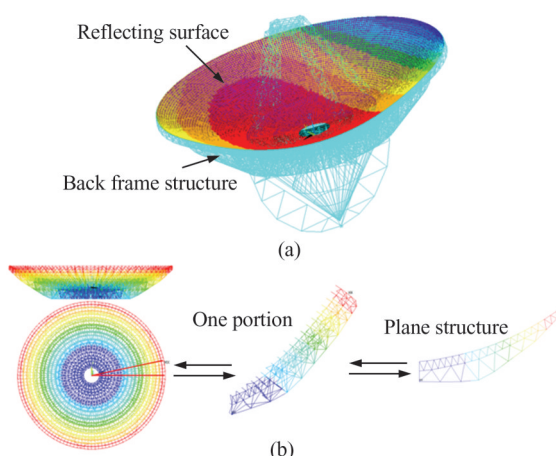


Fig. 19 Telescope (a) and back frame structure (b)

design. It uses carbon fiber material with a weight of 228.8 t. This structure is regarded as the back frame A, which is used for comparison with the back frame B designed by the force cone method.

### 2.2 Design of Back Frame B Based on Force Cone Method

Based on the mentioned force cone method above, the optimized back frame layout can be obtained by drawing. First, according to the specific design requirements of the back frame, the design domain boundaries, constraint points and load points are given, as shown in Fig. 21.

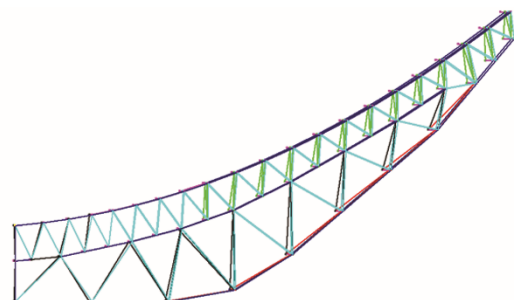


Fig. 20 One portion of the existing back frame A

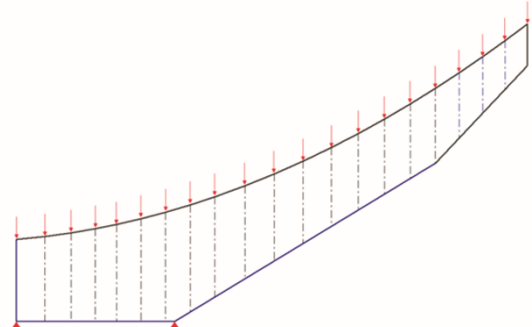


Fig. 21 Boundary conditions of the force cone method

The triangles represent the constraint points, and the upper arrow indicates the reflecting surface load on the back frame

If all load points above are considered into drawing the load force cones, the structure will be very complicated. Therefore, based on the specific situation, two simplifications are made as follows:

1) Combined with the "double-layer" idea in the design requirements, the load points indicated by the arrows are connected in groups of three to form a series of new load points, as shown in Fig. 22. This idea reduces the number of load points and simplifies the design. Additionally, it conforms to the design requirement of double-layer back frame.

2) The load force cones are not drawn, only the constraint force cones are drawn, and grow to the load points one by one.

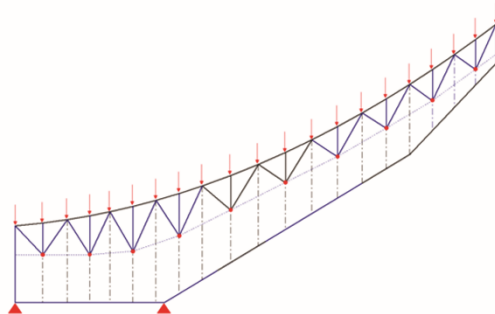


**Fig. 22 Simplification of the load points**

The triangles represent the constraint points, and the upper arrow indicates the reflecting surface load on the back frame

Based on the above conditions, draw the corresponding force cones according to the drawing rules of the force cone method, and the growth paths of the force cones are shown in Fig. 23. Connect the beams according to the corresponding force cone growth rules and do some fine adjustments to get the force cone back frame topology, as shown in Fig. 24. Using the same material and beam cross-section size as the above-mentioned existing back frame A, the weight of the back frame B ob-

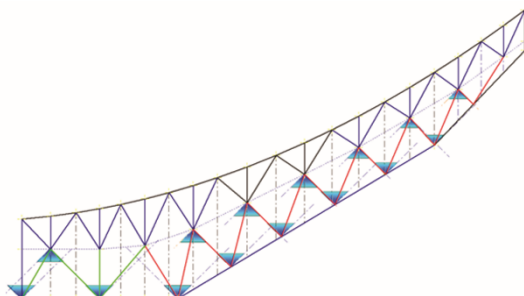


**Fig. 23 Growth paths of the force cones**

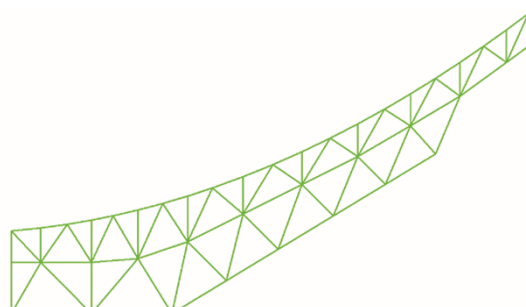


**Fig. 24 Topology of back frame B obtained by force cone method**

tained by the force cone method is 216.5 t.

### 3 Comparison of the Two Back Frames

The structural deformation, RMS and the stress of the back frame A and B are calculated and compared under the two typical gravity loading cases of  $90^\circ$  and  $0^\circ$ , as shown in Fig. 25.

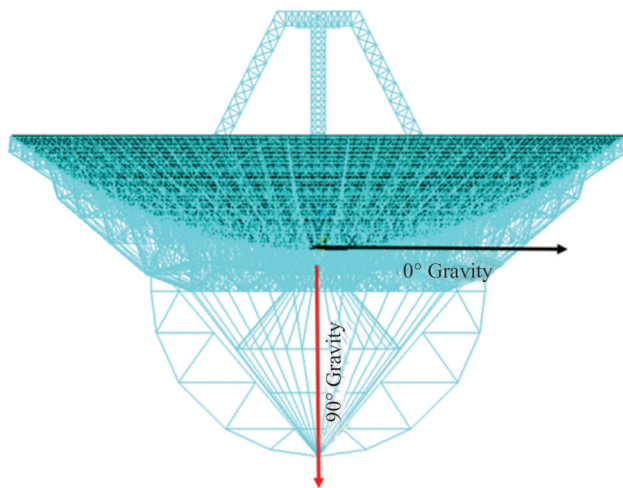


**Fig. 25 Calculation load cases**

#### 3.1 Results of $90^\circ$ Gravity Load Case

The deformation contours of the two back frame structures under  $90^\circ$  gravity load case are shown in Fig. 26. The maximum displacement of the existing back frame A is 5.43 mm, and the maximum displacement of the back frame B designed by the force cone method is 4.28 mm. The RMS calculation results are shown in Fig. 27. The RMS of back frame A is 0.149 mm, and the RMS of back frame B is 0.116 mm. The stress contours are shown in Fig. 28, and the stress scatter diagrams of back frame beams are shown in Fig. 29. The stress distribution of back frame A is  $-13.5\text{--}7.92$  MPa, and back frame B is  $-9.22\text{--}6.52$  MPa.

#### 3.2 Results of the $0^\circ$ Gravity Load Case

The deformation contours of the two back frame structures under  $0^\circ$  gravity load case are shown in Fig. 30. The maximum displacement of the existing back frame A is 25.5 mm, while for the back frame B it is 20.4 mm, as a comparison. The RMS calculation results are shown in Fig. 31. The RMS of back frame A is 1.47 mm, and the RMS of back frame B is 1.12 mm. The

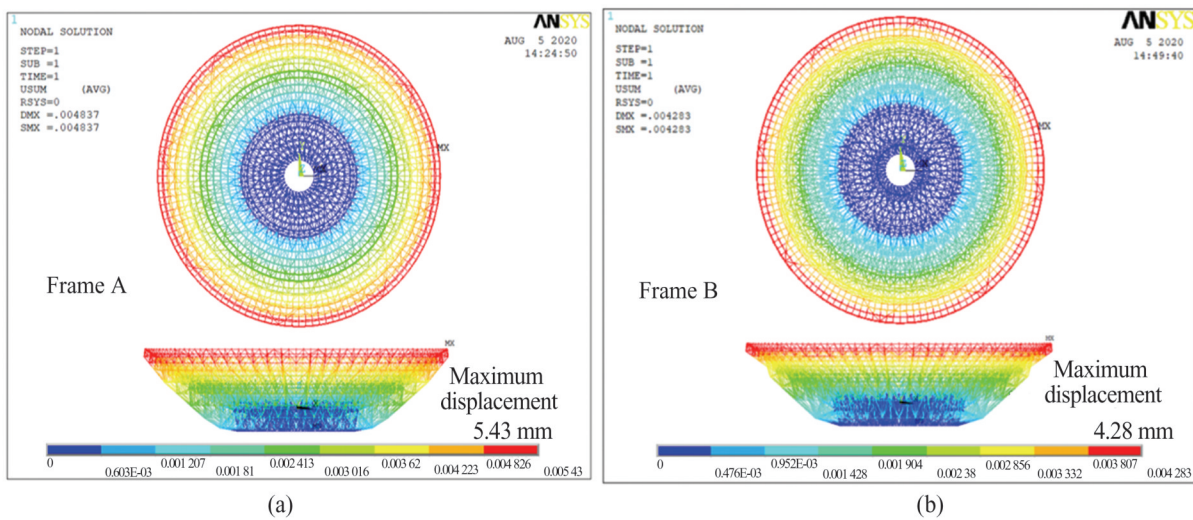


Fig. 26 Deformation contours of back frame A (a) and B (b) under 90° load case

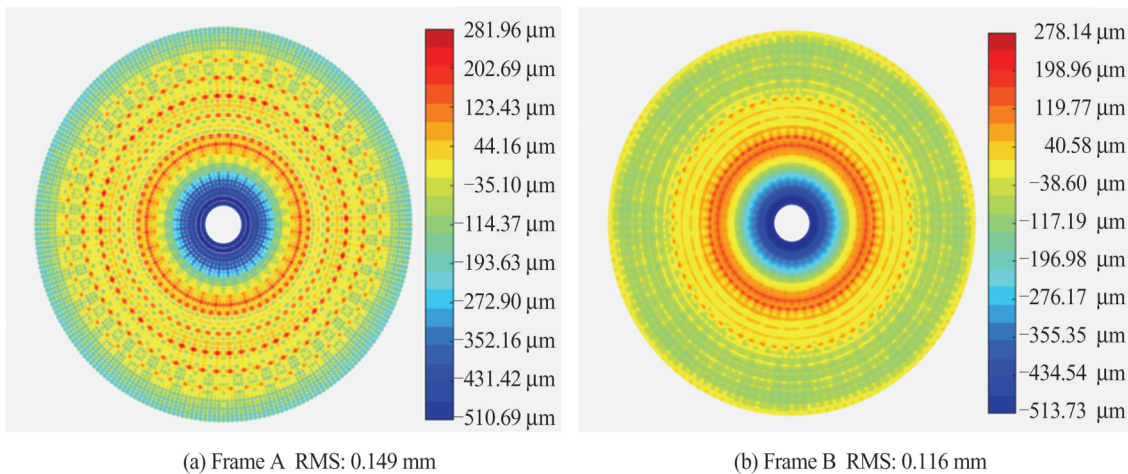


Fig. 27 RMS contours of back frame A (a) and B (b) under 90° load case

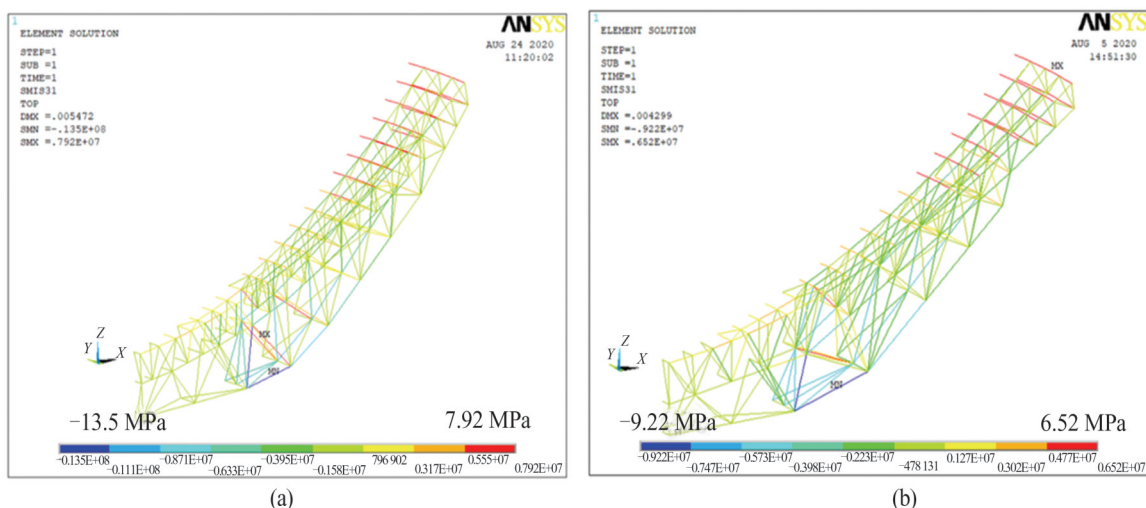


Fig. 28 Stress contours of one portion of back frame A (a) and B (b) under 90° load case

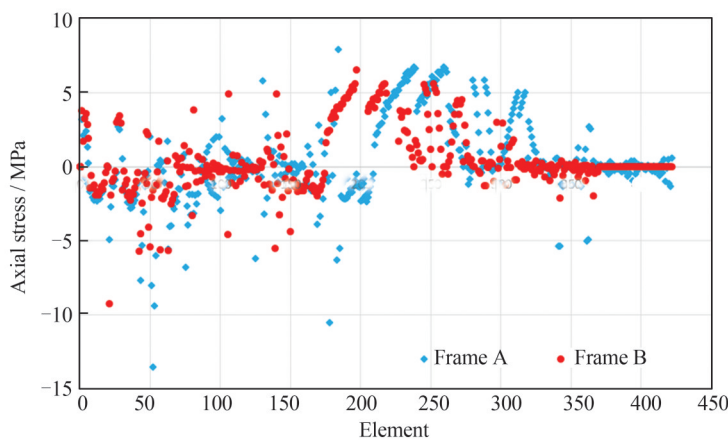


Fig. 29 Stress scatter diagrams of one portion of back frame A and B under 90° load case

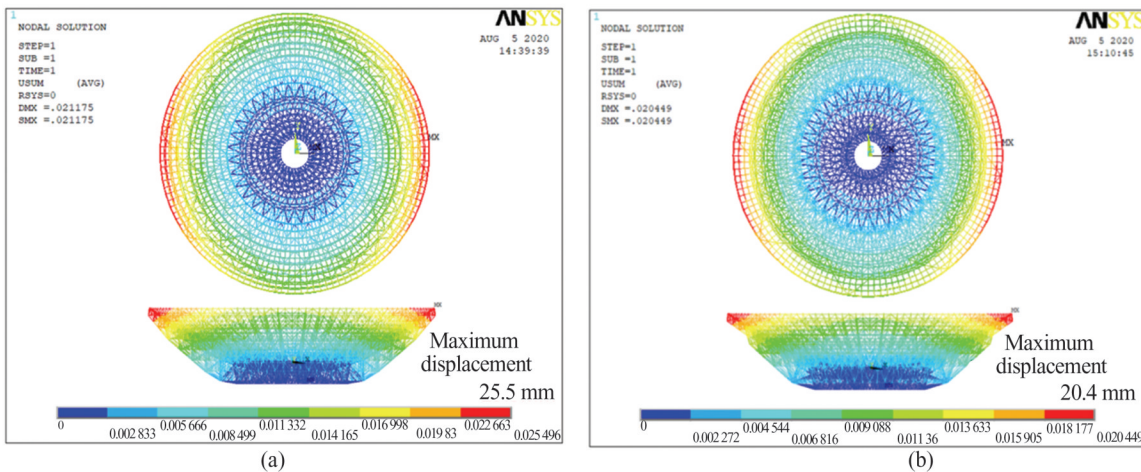


Fig. 30 Deformation contours of back frame A (a) and B (b) under 0° load case

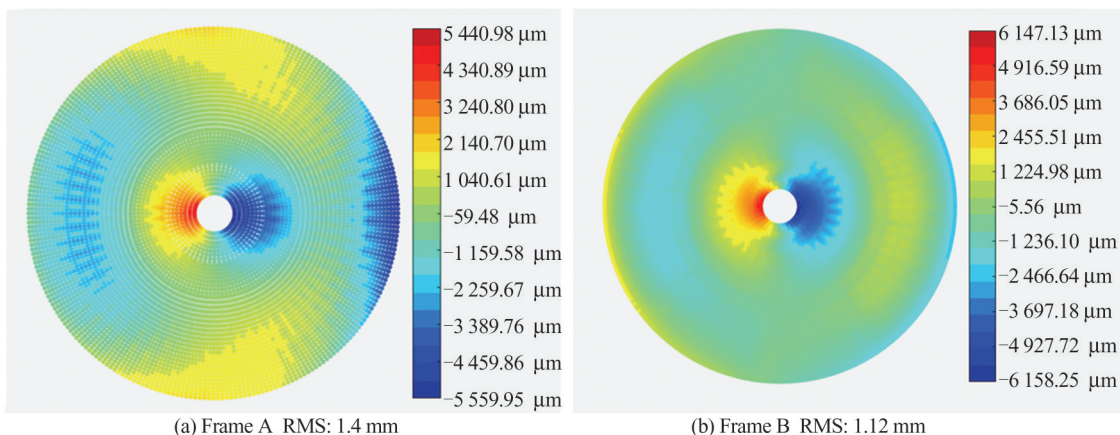


Fig. 31 RMS contours of back frame A (a) and B (b) under 0° load case

stress contours are shown in Fig. 32. The stress distribution of back frame A is -53 to 18.2 MPa, and back frame B is -41.7 to 15.1 MPa. The stress scatter diagrams of back frame beams are shown in Fig. 33.

### 3.3 Summary of the Comparison

Firstly, according to the weight comparison results, the weight of the back frame B designed by the force cone method is 216.5 t, while the weight of the existing

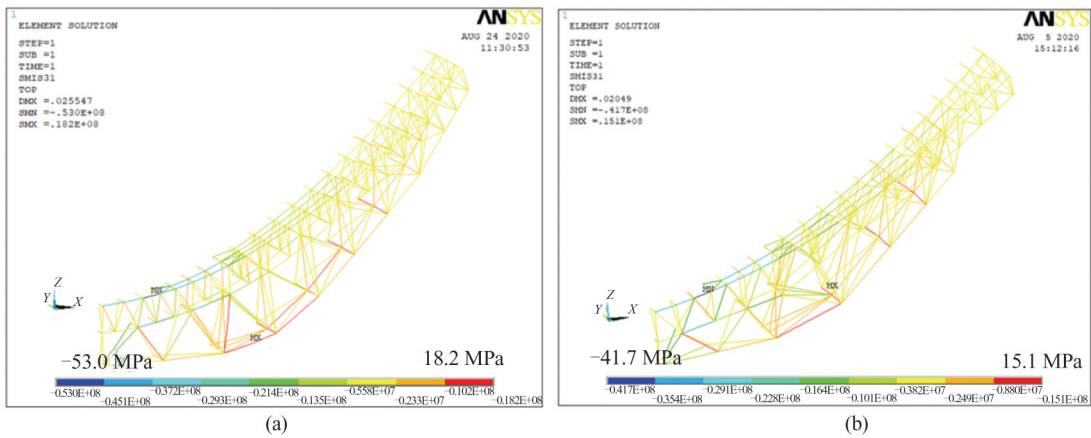


Fig. 32 Stress contours of one portion of back frame A (a) and B (b) under  $0^\circ$  load case

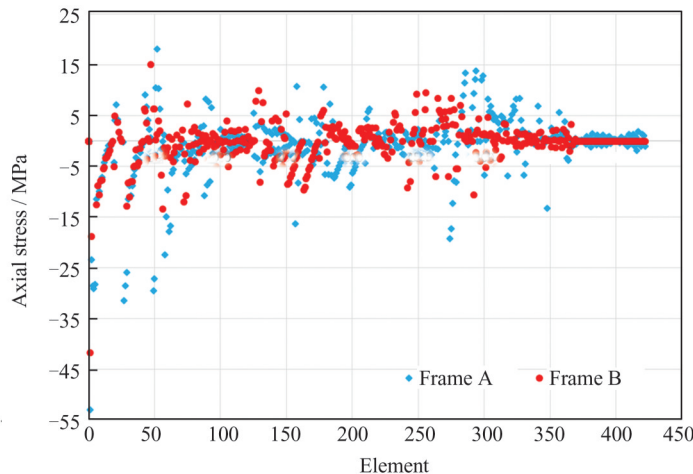


Fig. 33 Stress scatter diagrams of one portion of back frame A and B under  $0^\circ$  load case

back frame A is 228.8 t (reduced by 12.3 t, 5.4% of the original weight). Besides, through the comparison of the calculation results under two load cases, the back frame B has smaller deformation, higher stiffness and higher RMS precision than the existing back frame A even with lighter weight. What's more, the stress distribution of the beams in the back frame B is more uniform. After comprehensive consideration and comparison, the back frame B can be considered better than the existing back frame A, thus proves the effectiveness of the force cone growth method for truss structure design.

## 4 Conclusion

Based on the new conception of force cone, a force cone growth method for optimizing the topological layout of truss structure is proposed. Based on this method, the optimization design of the large radio telescope back

frame is carried out to obtain lightweight back frame structure with high stiffness, high precision and uniform stress. As a new method of truss structure optimization design, the force cone growth method is simple in theory and has high practical value. But at present, the force cone method is only suitable for two-dimensional truss layout optimization with simple boundary conditions, and further research is needed in the following aspects: 1) force cone growth method applicable to the optimization of 3D truss layout; 2) force cone growth method applicable to complex boundary conditions; 3) force cone growth method applicable to the optimization of large structures.

## References

- [1] von Hoerner S. Homologous deformations of tiltable tele-

- scopes [J]. *Journal of the Structural Division*, 1967, **93**: 461-486.
- [2] Chen S X, Ye S H. The accurate homologous design and optimization of antenna structure [J]. *Acta Mechanica Solida Sinica*, 1986(3): 189-197.
- [3] Levy R. Computer design of antenna reflectors [C]//14th *Structures, Structural Dynamics, and Materials Conference*. Reston: AIAA, 1973: 351.
- [4] Liu Y, Dai E B. Structural selection and accuracy control of the large aperture fully steerable antenna [J]. *The Structural Design of Tall and Special Buildings*, 2018, **27**(11): e1482.
- [5] Liu Y. *Structural Selection and Accuracy Control of the Large Aperture All-Movable Telescope* [D]. Harbin: Harbin Institute of Technology, 2013(Ch).
- [6] Sigmund O, Maute K. Topology optimization approaches [J]. *Structural and Multidisciplinary Optimization*, 2013, **48**(6): 1031-1055.
- [7] Guo X, Zhang W S, Zhang J, et al. Explicit structural topology optimization based on moving morphable components (MMC) with curved skeletons[J]. *Computer Methods in Applied Mechanics and Engineering*, 2016, **310**: 711-748.
- [8] Du B X, Zhao Y, Yao W, et al. Multiresolution isogeometric topology optimisation using moving morphable voids [J]. *Computer Modeling in Engineering & Sciences*, 2020(3): 1119-1140.
- [9] Li H, Grandhi R V, Kobayashi M. Level-set based cellular division method for structural shape and topology optimization [C]//2018 *AIAA/ASCE/AHS/ASC Structures, Structural Dynamics, and Materials Conference*. Reston: AIAA, 2018: 1387.
- [10] Rahman K, Geni M. Bionic topology optimization method for continuum structures based on bone remodeling mechanism [J]. *Transactions of the Chinese Society for Agricultural Machinery*, 2014, **45**(5): 340-346(Ch).
- [11] Liu Y. Back frame structure optimization of large radio telescope [J]. *Computer Engineering and Design*, 2015, **36**(9): 2596-2601(Ch).
- [12] Qian H L, Fan F, Mao C, et al. Form selection and optimization of FAST back-structure [J]. *Journal of Harbin Institute of Technology*, 2010, **42**(4): 546-549(Ch).
- [13] Zhao Q, Atad-Ettedgui E, Lemke D, et al. Analysis, optimization, and modification the back-structure of FAST [J]. *Proc Spie*, 2008, **9**: 123-125.
- [14] Jiang D J, Zhang Z M. A review on topology and layout optimization of truss structures [J]. *Advances in Science and Technology of Water Resources*, 2006, **26**(2): 81-86(Ch).
- [15] Michell A G M. LVIII. The limits of economy of material in frame-structures [J]. *The London, Edinburgh, and Dublin Philosophical Magazine and Journal of Science*, 1904, **8**(47): 589-597.
- [16] Guo P F, Han Y S, Wei Y G. Imitate full-stressed design method of discrete variable structure [J]. *Engineering Mechanics*, 2000(1): 94-98(Ch).
- [17] Wu Q L, Zhou Q C, Xiong X L, et al. Layout and sizing optimization of discrete truss based on continuum [J]. *International Journal of Steel Structures*, 2017, **17**(1): 43-51.
- [18] Mattheck C, Haller S. The force cone method: A new thinking tool for lightweight structures [J]. *International Journal of Design & Nature and Ecodynamics*, 2013, **8**(2): 165-171.

